ACS APPLIED NANO MATERIALS

www.acsanm.org Article

Silica-Coated ZnS Quantum Dots for Multicolor Emission Tuning from Blue to White Light

Gerardo Saavedra Rodriguez, Raul Sanchez-Zeferino, Christian Chapa, and Mario Enrique Alvarez Ramos*

Cite This: *ACS Appl. Nano Mater.* 2021, 4, 12180−12187 Read Online

ACCESS | Metrics & More | Article Recommendations | Supporting Information

ABSTRACT: The present work reports the easy tunability from blue to cold-white light emission of ZnS quantum dots embedded into a silica matrix ($ZnS@SiO_2$) by simple heating treatments (up to 900 °C) without the need of rare earth or heavy metal ion doping. The heating causes gradual changes in the composition of samples, such as crystallization of cristobalite and formation of zinc silicate, whose optical properties contribute to the tunability of the material. The evolution of the induced changes in the shape and structure was followed by scanning electron microscopy, X-ray diffraction, X-ray photoelectron spectroscopy, and Raman and Fourier transformed infrared spectroscopies. Diffuse reflectance and photoluminescence spectroscopies were used to analyze the optical properties of the obtained materials, exhibiting that as-synthesized $ZnS@SiO_2$ nanoparticles have an intense and wide blue emission band centered around 440 nm under 325 nm excitation, which is modified by the temperature with the enhancement of the intensity and widening of the band emission, as well as maximum shifting. The calculations of the CIE 1931 chromaticity coordinates show the tuning of the precepted tonality of the emission color from ocean-blue (0.18, 0.14) up to blue-sky (0.20, 0.31) and cold white light (0.27, 0.33) with a correlated color temperature of 12 500 and 7400 K for the last two. Besides suitable and facile tuning of the color emission, the thermal treatment of samples increases the stability of each one allowing their long-term usage as emitting devices.

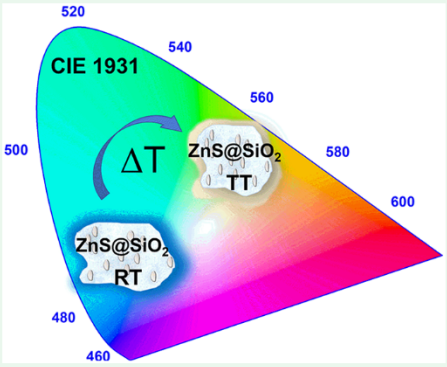

KEYWORDS: *Zinc sulfide, Quantum dots, Thermal treatment, Emission tuning, Luminescence, Nanophosphors*

INTRODUCTION

Nanostructured semiconductor materials have been widely studied during the last few years with great interest in their customizable electrical and optical properties. These properties, the optical one in particular, can be modified by controlling the size and shape of nanostructures and/or adding suitable doping ions. Since nanotechnology has allowed controlling the growth process of nanosystems, different semiconductor nanostructures of the II−VI group have been studied, especially quantum dots of ZnS, CdS, CdTe, CdSe, ZnTe, and so forth for many optoelectronic applications development,[1−9] such as light-emitting diodes,[10−16] whose emission is in the 400−640 nm spectral range with the possible tuning by using appropriately the quantum confinement effect and well-designed multilayered nano-semiconductor heterostructures.[8,17,18]

The zinc-based II−VI semiconductor nanoparticles and quantum dots, normally have high bandgap values, allowing these systems to produce blue light emissions, while the nanostructures without zinc lack photon emissions below 500 nm, that is, they are limited to produce green, yellow, or red light because of their smaller bandgap values.[11,15,17,19−22] Using zinc-based nanostructures, because of their blue light emissions, allows the development of tunable light devices by modifying their optical properties through doping with re or green-emitting ions, such as rare earth ions or Mn^{2+},[23−28] facing the challenge of introducing heavy and bigger ions into small nanoparticle's structure. But the alteration of optical properties of nanoparticles through thermal treatment is not explored widely; only a few works are studying the emission via heating processes on nanoparticles and quantum dots.[29−32]

Commonly, ZnS nanostructures have been synthesized using chemical routes, such as chemical bath deposition, precipitation, and solvothermal route, using polymers, silica, and other materials to stabilize them.[21,33−36] Also the silica photoemission is normally in the blue range and adds to the quantum dot systems many versatile improvements, such as stability against the photodegradation, weather humidity,

Received: August 27, 2021
Accepted: October 22, 2021
Published: November 4, 2021

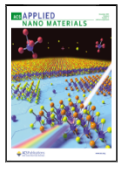

retention of optical properties of embedded nanoparticles, and so forth.[21,37−40]

The present work studies ZnS nanoparticles embedded into a silica matrix and their thermal transformation for multicolor light emission and the tunability of their photoluminescence emission from blue to cold-white light, obtained by simple heating treatments (up to 900 °C). The encapsulation into the silica matrix allows the preservation of the optical properties during the drying process to obtain powders because the ZnS nanoparticles remain fixed into the silica but insulated with respect to other ZnS nanoparticles. Their properties and thermal evolution were analyzed utilizing scanning electron microscopy (SEM), X-ray diffraction (XRD), X-ray photoelectron spectroscopy (XPS), Raman spectroscopy, Fourier transform infrared spectroscopy (FT-IR), diffuse reflectance spectroscopy (DRS), and photoluminescence (PL) spectroscopy. The photoluminescence emission of samples has been tuned by the modification of interband defects, the formation of additional crystalline phases of the existing materials, and the generation of new compounds as an effect of the temperature. An advantage of these nanophosphors is that they are obtained as powder, allowing the potential application of dry phosphors-based devices. Besides suitable tuning of the color of the light emission, the thermal treatment of samples increases the stability of each one, allowing their long-term usage as emitting devices.

EXPERIMENTAL DETAILS

Zinc nitrate hexahydrate [$Zn(NO_3)_2{\cdot}6H_2O$, >98%], sodium sulfide nonahydrate ($Na_2S{\cdot}9H_2O$, ≥98), tetraethyl orthosilicate, TEOS, [$Si(OC_2H_5)_4$, ≥98%], and cetyltrimethylammonium bromide (CTAB, ≥99%), all of analytical grade, were purchased from Sigma-Aldrich, Mexico, and used as precursors without further processing. Deionized (DI) water from a Milli Q system and Ethanol (CH_3CH_2OH, ≥99.8%) were used as solvent for reactions, as well as for washing the materials.

Silica-coated ZnS quantum dots ($ZnS@SiO_2$) were synthesized by a two-step one-pot method. For the first step, two ethanolic solutions of zinc nitrate (35 mL, 2.8 mM) and sodium sulfide (2.8 mM, 30 mL of ethanol, and 5 mL of DI) were independently prepared and mixed under high stirring and left reacting for 10 min. After the elapsed reaction time, the second step began by adding 35 mL of an additional ethanolic solution of CTAB (4 mM) and TEOS (1 mM) and placing the resulting solution into a Branson 3510R (100 W at 42 kHz) ultrasonic bath and left to react for 4 h. All of the products were washed at least five times (alternately with DI and ethanol), collected by centrifugation (31 000×*g*, 10 min), and dried at 70 °C for 8 h to obtain whitish powders, which were separated into nine samples, subjecting them to different thermal treatments (S1 = untreated, S2−S9 from 200 to 900 °C) during 2 h with a heating ramp rate of 10 °C/min.

The obtained $ZnS@SiO_2$ samples were characterized to study their morphology, structure, and optical properties. Scanning electron microscopy (SEM) and transmission electron microscopy (STEM) images of the samples were recorded in a JEOL JSM-7800F and JEM-2010F, respectively. X-ray diffraction (XRD) patterns were recorded using a PANalytical X'Pert MRD PRO device with a Cu-kα source (λ = 1.5406 Å) operating at 40 kV and 30 mA at a scanning rate of 0.1° (2θ s^{-1}) from 10 to 80° 2θ. Raman spectra were acquired using a Horiba LabRam 800 spectrometer, the excitation source was a He−Ne laser (λ = 632.8 nm), and the detector was a charge-coupled device (CCD). Fourier transform infrared (FT-IR) spectra were acquired using a PerkinElmer Spectrum Two FT-IR Spectrometer in attenuated total reflectance (ATR) mode. Room-temperature photoluminescence (PL) spectra of the samples were recorded in a Horiba iHR-320 spectrofluorometer, utilizing a 1200/500 grating and ambient-cooled Hamamatsu R928(P) multialkali photomultiplier tube (PMT) as the detector. Emissions from a 450 W Xe arc lamp and a 325 nm He−Cd laser line with the maximum incident power of 5 mW were utilized for sample excitation. Diffuse reflectance spectroscopy (DRS) spectra of the samples were recorded in a Perkin Elmer Lambda 365 UV−vis spectrophotometer coupled with an integrating sphere accessory. The spectra of X-ray photoelectron spectroscopy (XPS) were acquired using a Perkin Elmer PHI5100 spectrometer with Mg anode with an energy of 1240 eV.

RESULTS AND DISCUSSION

The room-temperature synthesized nanomaterial must be formed by quasi-spherical ZnS quantum dots (QDs) embedded into an amorphous silica matrix, as suggested in Scheme 1. It is suggested that the ZnS nanoparticles are

Scheme 1. $ZnS@SiO_2$ Nanocomposite Formed by ZnS QDs Embedded into the Silica Matrix

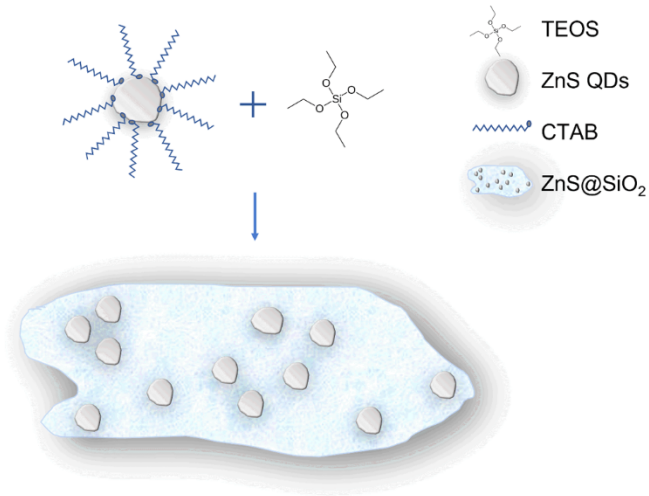

encapsulated during the formation of the silica network, serving as nucleation centers during the sol−gel process; the role of CTAB was to prevent big agglomerations of ZnS bare nanoparticles while the condensation and polymerization reaction of the silica occurred. Once the silica has formed, the ZnS nanoparticles must remain fixed and isolated from each other, avoiding the quenching of their optical properties in addition to their environmental degradation.[21] The ratio of TEOS with respect to zinc precursor was estimated based on the expected volume of products; the evaluated ratios were 1:1, 1:2, 1:3, and 1:5. The best results were obtained using the ratio of 1:3; given that when the silica thickness was thinner, the material did not withstand the heating, and when it was too big, the optical properties were not adequate.

In order to analyze the morphologies and the conformation of the synthesized samples, SEM and TEM images are presented in Figure 1, corresponding to the S1 sample. In the SEM image, at low magnification it is possible to observe that the material is constituted by agglomerated quasi-spherical-shaped nanoparticles with size below the 100 nm of diameter, while the TEM image at higher magnification shows that the material is formed by at least two different density materials that must be ZnS nanoparticles embedded into a silica matrix as we previously reported.[21] Although the silica exhibits an amorphous shape, the spherical ZnS nanoparticles are embedded into the matrix. In addition, Figure S1 shows an HRTEM micrograph which depicts the size and shape of the

https://doi.org/10.1021/acsanm.1c02689
ACS Appl. Nano Mater. 2021, 4, 12180−12187

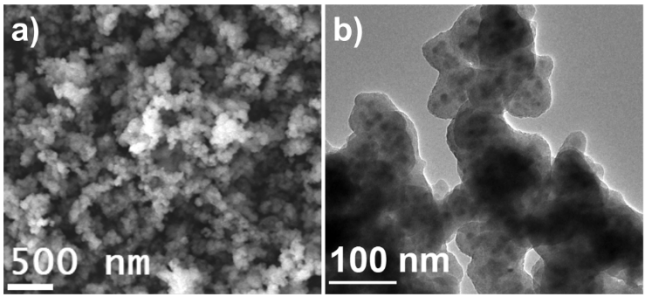

Figure 1. SEM and TEM micrographs of the S1 sample.

particles with more details, the electron diffraction pattern, and EDS spectrum of the sample.

Figure S2a–f shows low-magnification SEM images of S2–S7 samples. We cannot appreciate significant changes in size or shape of the particles, suggesting minor alterations in the microstructure of the samples by the temperature treatment. However, all of the images depict that the samples are conformed by quasi-spherical-shaped nanoparticles with a diameter smaller than 100 nm, as in the case of the S1 sample, which means that the microstructure of the material has good thermal stability.

The crystalline structure evolution of the synthesized materials was evaluated through XRD from 10 to 80° $2\theta°$, whose resulting patterns are shown in Figure 2. Figure 2a shows the patterns acquired from samples S1 to S7 and one pattern corresponding to our previous experimental result of bare ZnS quantum dots[21] that corresponds to a face-centered cubic (fcc) crystalline structure (zinc blende, PDF #00-05-0566), whose main peaks are around 28, 47, and 56 in $2\theta°$, corresponding to planes (111), (220), and (311), respectively. Considering that the ZnS nanostructures are enclosed into a sol–gel synthesized silica matrix, the corresponding patterns to the S's samples exhibit a major amorphous behavior. However, increasing the temperature of the thermal treatment (for the S1 to S5 samples), a clear trend toward increasing the presence of small signals that may correspond to ZnS peaks, corresponds with the mentioned positions. In the S6 sample, subjected to a higher temperature the ZnS signals disappear and change the shape of the band that corresponds to the amorphous silica, probably due to the beginning transformation of the material's phase and/or the formation of further compounds, which is observed in the pattern that corresponds to the S7 sample at a temperature of 700 °C, in which new peaks are observed, mounted in the silica band. These new peaks are well-defined at higher temperatures for S8 and S9 samples, shown in Figure 2b, exhibiting diffraction peaks corresponding to cristobalite-low (crystalline silica phase) and Zn_2SiO_4, comparing to the PDFs #01-075-0923 and #00-037-1485, respectively. These results imply that the crystallinity of the synthesized material is changing with the heating and the effect at the higher temperature being considered more, as expected. The higher temperature and the additional time that the heating and cooling ramps aggregate to the 2 h at the targeted set points above the 700 °C (800 and 900 °C), about 30 and 50 min, respectively, could explain these changes. Thus the diffraction patterns of S8 and S9 samples do not exhibit the amorphous silica behavior but show new well-defined signals that correspond to new crystalline phases as a consequence of heating.

In order to get more information about the evolution of the samples as the temperature increases below the 700 °C, an additional study was developed via X-ray photoelectron spectroscopy (XPS) to monitor the changes of the Zn $2p_{3/2}$ peak to determine the component compounds of the samples. The high-resolution spectra for these peaks were fitted using a pseudo-Voight function, 70% Gaussian and 30% Lorentzian; these values have been characterized for the instrument that we use, the minimum value of R^2 was 0.998, indicating the goodness of the fitting procedure. In Figure 3a, a survey spectrum of the S1 sample (untreated ZnS@SiO_2) is shown, where it is possible to observe signal peaks that correspond with the main components of the material, such as photoelectronic peaks $2p_{(1/2and3/2)}$ of the zinc atoms/ions, the 1s peak of the oxygen, the 2s and 2p peaks of the silicon, and some auger peaks. Because of the capping material, the sulfur 2p and 2s peaks can not be observed because of the nature of the technique, whose significative signals come from a maximum depth of 10 nm, being representative majorly of the surface. Figure S3 depicts the survey spectra of bare and silica capped ZnS nanoparticles, where the decrease of the photoelectronic signals is observed.

Figure 3b–d exhibits the high-resolution spectra of the Zn $2p_{3/2}$ photoelectronic peak from the S1 (b), S6 (c), and S7 (d) samples, all of them fitted with two components: the first one at 1021.8 eV of binding energy which corresponds to the Zn–S, while the second one at 1022.8 eV corresponds with zinc

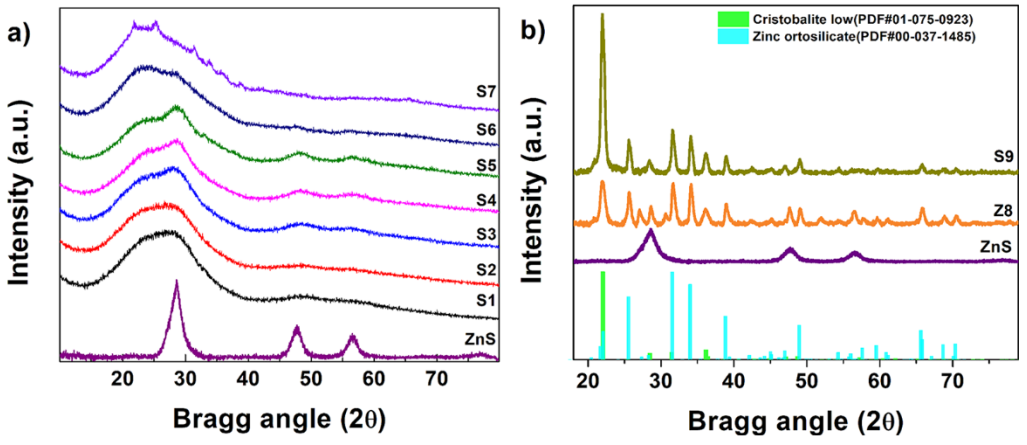

Figure 2. XRD patterns of the S1–S9 samples.

https://doi.org/10.1021/acsanm.1c02689
ACS Appl. Nano Mater. 2021, 4, 12180–12187

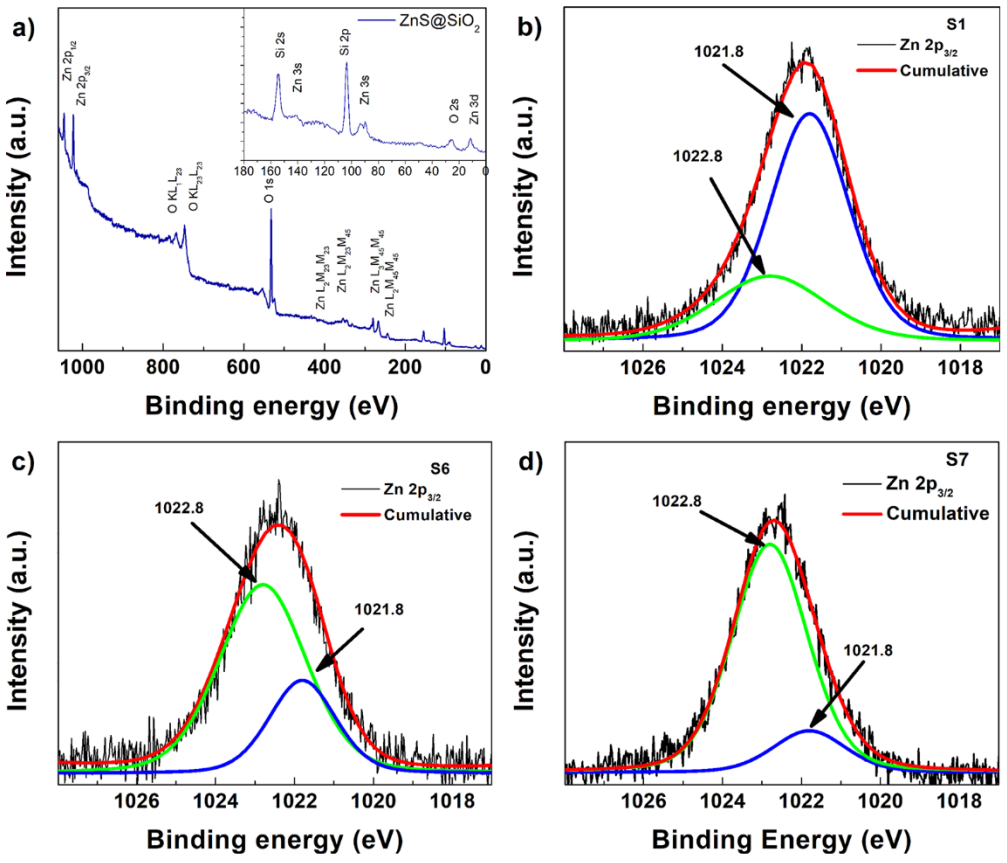

Figure 3. XPS survey (a) and high-resolution spectra of S1 (b), S6 (c), and S7 (d) samples where the evolution of their component are shown.

ions bound to silicate ion (SiO_4) in $ZnSiO_4$ samples.[41] On the one hand, with just the covering process of the ZnS nanoparticles with silicon dioxide the formation of different zinc compounds at the interaction zone of both materials occurred and was previously analyzed and reported.[21] On the other hand, their evolution against temperature has been followed by tracking the intensity rate of both main components that exhibit evidence of the gradual transformation from ZnS to $ZnSiO_4$ as the temperature increases. In the case of S2−S5 samples, they exhibit the same composition as the S1 sample with minor variations.

Raman spectra of the S1 and a ZnS sample synthesized as control in Figure S4a exhibit characteristic vibrational modes that correspond to a cubic Sphalerite type ZnS structure, whose main spectral values are found around 264 and 345 cm^{-1} (corresponding to the $E_1(TO)$ and $E_1(LO)$, respectively) that we also previously reported.[21] The differences between S1 and the control in intensity and the peak's fwhm can be attributed to the Zn−SiO_2 interactions and the isolation of ZnS particles due to the coating. $E_1(TO)$ displacement and the intensity changes of the $E_1(LO)$ and the multimode around 420 cm^{-1} of the nanocomposite can be explained considering a better dispersion and smaller size of the ZnS particles.[21,42] The differences observed between 400 and 500 cm^{-1} can be attributed to SiO_2 modes[21,43,44] and ZnS multimodes.[21,43,45] Unfortunately, the evolution of the Raman active modes was not possible to follow because of the phosphorescence of the heat-treated samples (S2−S9) and was necessary to develop a further vibrational characterization. The FTIR spectra of S1 and a synthesized SiO_2 sample, shown in Figure S4b, exhibit characteristic vibrational modes of the silica from 800 to 1300 cm^{-1}, the range of interest, corresponding to reported symmetric (1075 cm^{-1}) and asymmetric (800 cm^{-1}) stretching vibrational modes Si−O−Si.[46,47]

A further FT-IR analysis was performed to study the evolution of the material with the temperature, and their corresponding spectra are shown in Figure 4. From 1400 to 4000 cm^{-1}, in the uninterest range the signals are related to solvent and surfactant residues during the capping process,

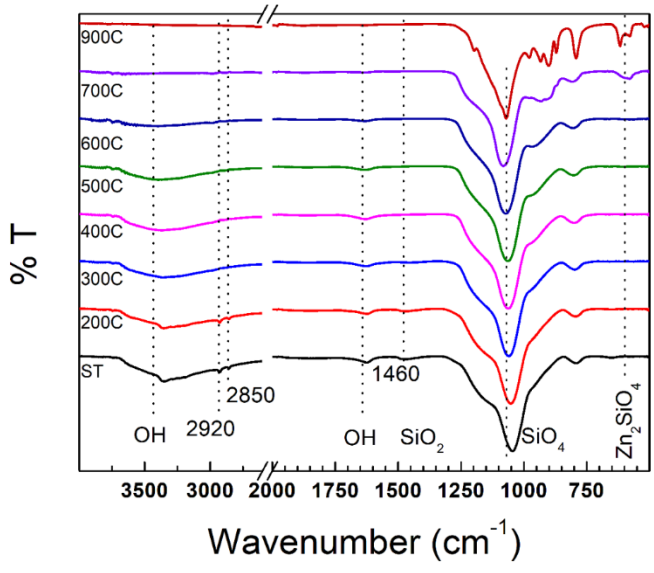

Figure 4. FT-IR spectra of the evolution of the ZnS@SiO_2 with thermal treatment at various temperatures.

https://doi.org/10.1021/acsanm.1c02689
ACS Appl. Nano Mater. 2021, 4, 12180−12187

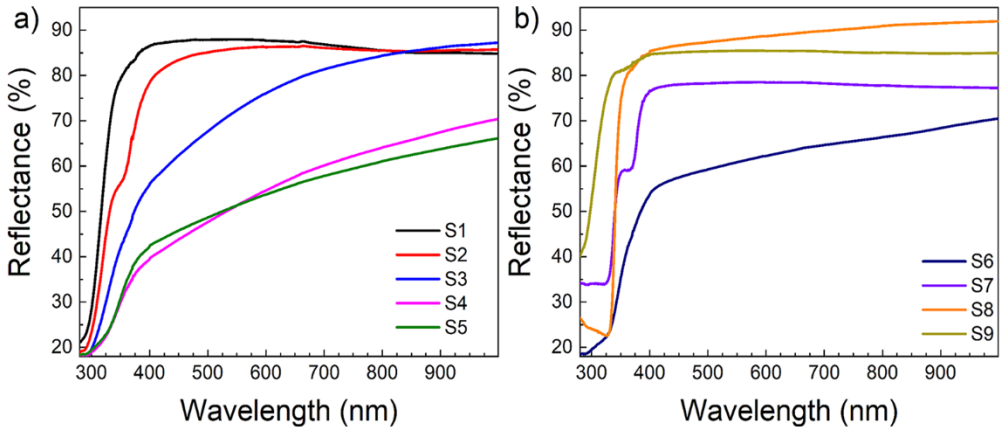

Figure 5. Diffuse reflectance spectra of the S1−S9 samples.

such as O−H vibrations of the water and ethanol or C−H vibrations of trapped CTAB (3000−4000 and 2850−2910 cm^{-1}, respectively), and they decrease as the temperature increases until they disappear. Into the interest range (500−1400 cm^{-1}) where the vibrational modes of silica appear, it is possible to observe a small position shifting in the main band around 1075 cm^{-1}, the enhancement of the intensity and definition as the temperature increases of a signal around 900 cm^{-1} related commonly with crystalline structures of silicon oxide ($SiOx$, $x = 4$ normally) and the appearing of a couple of signals around 600 cm^{-1} since 700 °C and higher temperatures, that has been reported for the Zn−O−Si vibrations for zinc (and other transition metal ions like titanium) orthosilicate ($ZnSiO_4$) and induced cristobalite formation.[48−51]

To acquire evidence of the evolution of the optical properties as the temperature increases, the diffuse reflectance spectra of all samples were collected in which was not possible to establish any certain trend considering all samples; However, by analyzing the spectra of Figure 5a that corresponds with the lower temperatures, the unique trending behavior is the decreasing of the reflectance percent in the visible range (400−700 nm), attributable to the possible generation of acceptor defects. In the case of the spectra shown in Figure 5b, they exhibit clear position shifts in the border edge also. In the case of samples S2, S7, and S9, it is possible to appreciate two borders that suggest that the material is not formed by a unique crystalline phase; in this case, the simple coating process induces the presence and interaction between multiple compounds (ZnS, $ZnSiO_4$, SiO_2, and so forth) and crystal phases (silica, cristobalite, for example) induced by the heating treatment that have a distinct optical bandgap and are in an uncertain percentage each, resulting in complex but interesting optical properties.

Figure S5 shows the steady-state PL spectra corresponding to the bare ZnS and S1 samples in which we can observe a wide blue emission band between 360 and 650 nm approximately with a maximum centered around 440 nm. The spectra were deconvoluted in four and five component Gaussian peaks, obtaining R^2 values above 0.998 for the cumulative curve, which are related to the luminescent transitions between defects into ZnS nanoparticles plus the silica self-defects and the inherent interactions between both materials. In the case of ZnS nanoparticles, these multiple defect transitions can be sulfur vacancies, near band-edge levels, zinc interstitials, and their combinations, as we have previously analyzed and reported.[21] The luminescence in silica glass has been well studied and mainly associated with the bridging or nonbridging oxygen (BO and NBO, respectively);[53] thus in the interaction zone (interface between the surface of ZnS nanoparticle and capping silica), the number of defects increases, resulting in a higher number of "luminescent sources."

In Figure 6, the changes in the photoluminescence properties are shown as a consequence of the observed evolution in the sample components induced by the heating temperature, and the changes of the maximum intensity are shown in the figure (blue numbers). Compared with the spectrum of the S1 sample, the one corresponding to the S2 sample does not exhibit significant spectral changes, such as band widening or maximum position shifting, which implies changes in the rate between components of the emission, but an intensity enhancement is induced and probably associated with the trapped solvent evaporation and the densification of the silica, as suggested in the previous DRS and FT-IR discussion. From 300 to 600 °C (S3, S4, S5, and S6 samples), more significant changes are observed in the spectral shape of the emission, principally the enhancement and broadening of the emission component around 530 nm that is due to the self-defects of the ZnS nanoparticles, oxidation at their surface, densification of the silica, and the formation of other compounds such as the zinc silicate determined by XPS and FT-IR.[28,48,52] Also, major changes in the spectral properties of the samples were subjected to thermal treatment from 700 to 900 °C (S7, S8, and S9 samples) with respect to S1, such as the absence of the component around 400 nm and the narrowing of the emission bands around 440 and 530 nm with their respective changes in intensity; all of these changes were produced by the formation of well-defined crystalline phases, as was found in XRD patterns, which have been reported with blue[48,53] and green[28,52] emission properties.

Evaluating the spectra of all samples with the standard CIE 1931 allows for the calculation of the (x,y) chromaticity coordinates by weighting each spectrum with the empiric tristimulus functions of the response of human eyes and placing them into the color diagram shown in Figure 7. The specific coordinates of each sample are labeled in the figure and correspond with the color perception of our eyes of their global emission. Samples S1 and S2 exhibit a blue emission color with (0.18, 0.14) and (0.18, 0.17) chromaticity coordinates, respectively, and from this point the thermal treatment induces the color change until a near white zone for

https://doi.org/10.1021/acsanm.1c02689
ACS Appl. Nano Mater. 2021, 4, 12180−12187

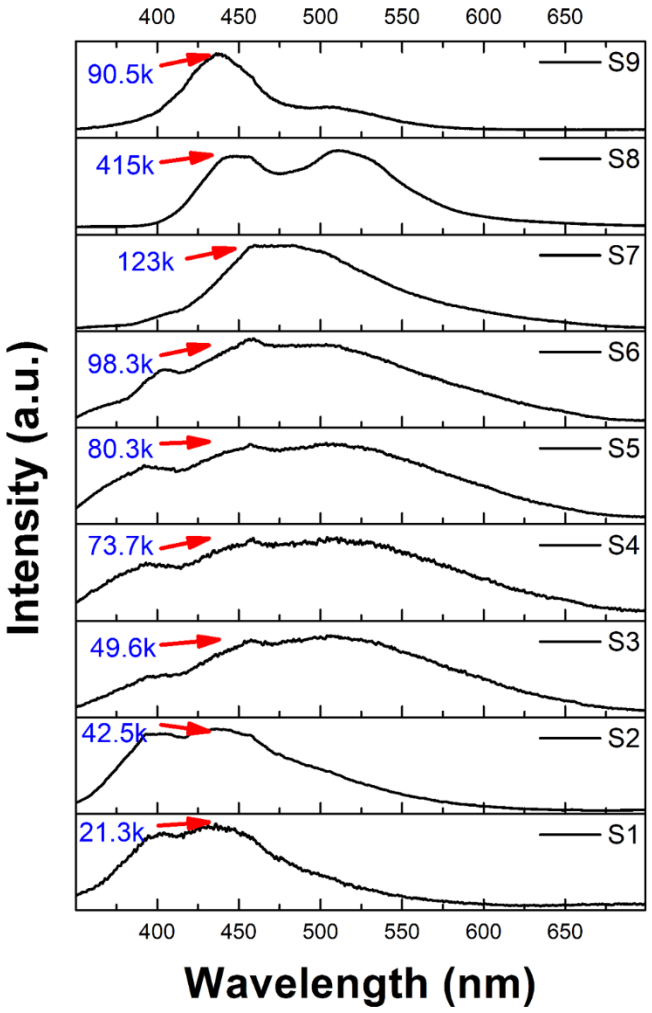

Figure 6. Photoluminescent spectra of S1−S9 samples under 325 nm excitation.

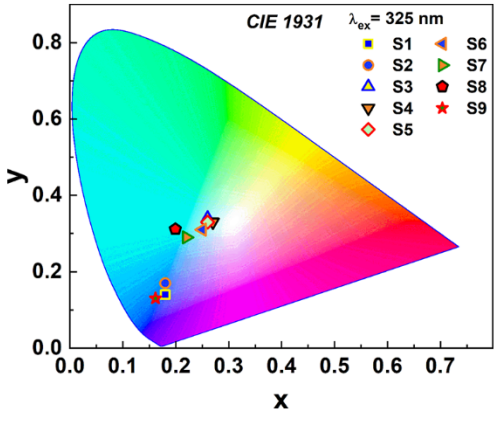

Figure 7. CIE chromaticity coordinates of the S1−S9 samples.

samples S3, S4, S5, and S6, whose chromaticity coordinates are listed in Table 1. In the case of the higher heating temperature, the emission colors are displaced to a greenish-blue for samples S7 and S8, caused by the increasing green and blue emissions of the growing new phases into the material, until a return to the blue for sample S9 because of the predomination of blue-emitting crystalline phases.

Table 1. Chromaticity Coordinates and CCT of the Emissions

sample	x	y	CCT
S1	0.18	0.14	
S2	0.18	0.17	
S3	0.26	0.34	7785
S4	0.27	0.33	7428
S5	0.26	0.33	7932
S6	0.25	0.31	8914
S7	0.22	0.29	12033
S8	0.20	0.31	12529
S9	0.16	0.13	

In order to explore further colorimetric characteristics of the wide tunable emissions, the correlated color temperature (CCT) for the S3 to S8 samples was calculated, and performing the calculations for samples S1, S2, and S9 would not make sense because CCT would be extremely high. For the calculation of CCT, McCammy's equation was used[54]

$$\mathrm{CCT} = -449n^3 + 3525n^2 - 6823.3n + 5522.21 \quad (1)$$

where $n = (x_s - x_e)/(y_s - y_e)$ is the reciprocal slope between the formed line from the sample point with chromaticity coordinates (x_s,y_s) and the point $(x_e = 0.3134, y_e = 0.1543)$ where the iso-temperature lines in the Planckian locus converge, which represents the tangent of the angle formed between the y-axis and this line. The CCT results are listed in Table 1, which correspond to cold-white (day light) for S3, S4, S5, and S6. For the emission color of S7 and S8, the CCT values correspond to blue-sky light.

CONCLUSIONS

A simple route was used to synthesize ZnS@SiO_2 nanopowders, consisting of ZnS quasi-spherical nanoparticles embedded into a silica matrix. The material was subjected to thermal treatments varying the temperature from 200 to 900 °C, observing significant changes in their optical properties due to the formation of new phases and new compounds as the temperature increases, which presence was determined through XRD, XPS, and FT-IR characterizations.

Using the PL spectra, the chromaticity coordinates were calculated, which exhibit the tunability of the emission color from blue to white (blue-sky and day-light tonalities) as a result of the evolution of the optical properties induced by the thermal treatment. Through McCamy's formulation, the CCT was calculated for the samples that exhibit emission colors near the white light in which values are used to compare a light source with known sources like day light for illumination purposes. Although the composition of samples is changing, the optical properties are stable and suitable for developing light-emitting devices with different colors, and the higher temperatures of thermal treatment ensure that the material has good stability for long-term applications. Another advantage of these nanophosphors is that they are obtained as powders because many QDs-based materials have great properties in solution but lose them when dried.

ASSOCIATED CONTENT

Supporting Information

The Supporting Information is available free of charge at https://pubs.acs.org/doi/10.1021/acsanm.1c02689.

Additional figures (PDF)

https://doi.org/10.1021/acsanm.1c02689
ACS Appl. Nano Mater. 2021, 4, 12180−12187

AUTHOR INFORMATION

Corresponding Author

Mario Enrique Alvarez Ramos − *Departamento de Física, Universidad de Sonora, Hermosillo, Sonora 83000, Mexico;* orcid.org/0000-0001-7598-9683; Email: mario@alvarez.uson.mx

Authors

Gerardo Saavedra Rodriguez − *Departamento de Física, Universidad de Sonora, Hermosillo, Sonora 83000, Mexico;* orcid.org/0000-0002-6608-787X

Raul Sanchez-Zeferino − *Departamento de Física, Universidad de Sonora, Hermosillo, Sonora 83000, Mexico;* orcid.org/0000-0002-2256-6836

Christian Chapa − *Instituto de Intenieria y Tecnología de la Universidad Autónoma de Ciudad Juárez, Chihuahua 32310, Mexico*

Complete contact information is available at: https://pubs.acs.org/10.1021/acsanm.1c02689

Notes

The authors declare no competing financial interest.

ACKNOWLEDGMENTS

G.S. would like to thank Consejo Nacional de Ciencia y Tecnología (CONACyT), México, for offering a graduate scholarship. The authors acknowledge funding from (CONACyT) México, through Grants INFR-255791-2015 and INFR-226208-2014. The authors gratefully acknowledge the Transmission Electron Microscope Laboratory of the University of Sonora, for extending TEM facilities utilized in this work.

REFERENCES

(1) Bondar, N. V.; Brodyn, M. S. Evolution of Excitonic States in Two-Phase Systems with Quantum Dots of II-VI Semiconductors near the Percolation Threshold. *Phys. E (Amsterdam, Neth.)* **2010**, *42* (5), 1549−1554.

(2) Yu, Y.; Xu, L.; Chen, J.; Gao, H.; Wang, S.; Fang, J.; Xu, S. Hydrothermal Synthesis of GSH-TGA Co-Capped CdTe Quantum Dots and Their Application in Labeling Colorectal Cancer Cells. *Colloids Surf., B* **2012**, *95*, 247−253.

(3) Li, H.; Shih, W. Y.; Shih, W. H. Non-Heavy-Metal ZnS Quantum Dots with Bright Blue Photoluminescence by a One-Step Aqueous Synthesis. *Nanotechnology* **2007**, *18* (20), 205604.

(4) Ozgur, U.; Alivov, Y. I.; Liu, C.; Teke, A.; Reshchikov, M. A.; Dogan, S.; Avrutin, V.; Cho, S.-J.; Morkoc, H. A Comprehensive Review of ZnO Materials and Devices. *J. Appl. Phys.* **2005**, *98* (4), 041301.

(5) Rohlfing, M.; Krüger, P.; Pollmann, J. Role of Semicore Electrons in Quasiparticle Band-Structure Calculations. *Phys. Rev. B: Condens. Matter Mater. Phys.* **1998**, *57* (11), 6485−6492.

(6) Su, G.; Liu, C.; Deng, Z.; Zhao, X.; Zhou, X. Size-Dependent Photoluminescence of PbS QDs Embedded in Silicate Glasses. *Opt. Mater. Express* **2017**, *7* (7), 2194.

(7) Seo, Y. S.; Justin Raj, C.; Kim, D. J.; Chul Kim, B.; Yu, K. H. Effect of CdSe/ZnS Quantum Dots Dispersion in Silicone Based Polymeric Fluids. *Mater. Lett.* **2014**, *130*, 43−47.

(8) Sookhakian, M.; Amin, Y. M.; Basirun, W. J.; Tajabadi, M. T.; Kamarulzaman, N. Synthesis, Structural, and Optical Properties of Type-II ZnO-ZnS Core-Shell Nanostructure. *J. Lumin.* **2014**, *145*, 244−252.

(9) Naughton, M. S.; Kumar, V.; Bonita, Y.; Deshpande, K.; Kenis, P. J. A. High Temperature Continuous Flow Synthesis of CdSe/CdS/ZnS, CdS/ZnS, and CdSeS/ZnS Nanocrystals. *Nanoscale* **2015**, *7* (38), 15895−15903.

(10) Kamat, P. V. Quantum Dot Solar Cells. The next Big Thing in Photovoltaics. *J. Phys. Chem. Lett.* **2013**, *4* (6), 908−918.

(11) Janssen, R. A. J.; Stouwdam, J. W. Red, Green, and Blue Quantum Dot LEDs with Solution Processable ZnO Nanocrystal Electron Injection Layers. *J. Mater. Chem.* **2008**, *18* (16), 1889−1894.

(12) Minot, E. D.; Kelkensberg, F.; Van Kouwen, M.; Van Dam, J. A.; Kouwenhoven, L. P.; Zwiller, V.; Borgström, M. T.; Wunnicke, O.; Verheijen, M. A.; Bakkers, E. P. A. M. Single Quantum Dot Nanowire LEDs. *Nano Lett.* **2007**, *7* (2), 367−371.

(13) Liu, Y.-Q.; Zhang, D.-D.; Wei, H.-X.; Ou, Q.-D.; Li, Y.-Q.; Tang, J.-X. Highly Efficient Quantum-Dot Light Emitting Diodes with Sol-Gel ZnO Electron Contact. *Opt. Mater. Express* **2017**, *7* (7), 2161−2167.

(14) Zhang, Q.; Nie, C.; Chang, C.; Guo, C.; Jin, X.; Qin, Y.; Li, F.; Li, Q. Highly Luminescent Red Emitting CdZnSe/ZnSe Quantum Dots Synthesis and Application for Quantum Dot Light Emitting Diodes. *Opt. Mater. Express* **2017**, *7* (11), 3875−3884.

(15) Shen, H.; Bai, X.; Wang, A.; Wang, H.; Qian, L.; Yang, Y.; Titov, A.; Hyvonen, J.; Zheng, Y.; Li, L. S. High-Efficient Deep-Blue Light-Emitting Diodes by Using High Quality ZnxCd1-XS/ZnS Core/Shell Quantum Dots. *Adv. Funct. Mater.* **2014**, *24* (16), 2367−2373.

(16) Jin, X.; Bai, J.; Gu, X.; Chang, C.; Shen, H.; Zhang, Q.; Li, F.; Chen, Z.; Li, Q. Efficient Light-Emitting Diodes Based on Reverse Type-I Quantum Dots. *Opt. Mater. Express* **2017**, *7* (12), 4395−4407.

(17) Caruge, J. M.; Halpert, J. E.; Wood, V.; Bulovic, V.; Bawendi, M. G. Colloidal Quantum-Dot Light-Emitting Diodes with Metal-Oxide Charge Transport Layers. *Nat. Photonics* **2008**, *2* (4), 247−250.

(18) Chukwuocha, E. O.; Onyeaju, M. C.; Harry, T. S. T. Theoretical Studies on the Effect of Confinement on Quantum Dots Using the Brus Equation. *World J. Condens. Matter Phys.* **2012**, *02* (02), 96−100.

(19) Zhang, W. J.; Pan, C. Y.; Cao, F.; Yang, X. White-Light-Emitting Cu,Mn Co-Doped Zn-In-S/ZnS Quantum Dots with High Stability and Their Electroluminescence. *J. Mater. Chem. C* **2017**, *5* (40), 10533−10542.

(20) Wang, C.; Xu, S.; Wang, Y.; Wang, Z.; Cui, Y. Aqueous Synthesis of Multilayer Mn:ZnSe/Cu:ZnS Quantum Dots with White Light Emission. *J. Mater. Chem. C* **2014**, *2* (4), 660−666.

(21) Saavedra Rodríguez, G.; Carrillo Torres, R. C.; Sánchez Zeferino, R.; Álvarez Ramos, M. E. Stabilized Blue Emitting ZnS@SiO 2 Quantum Dots. *Opt. Mater. (Amsterdam, Neth.)* **2019**, *89*, 396−401.

(22) Fang, X.; Zhai, T.; Gautam, U. K.; Li, L.; Wu, L.; Bando, Y.; Golberg, D. ZnS Nanostructures: From Synthesis to Applications. *Prog. Mater. Sci.* **2011**, *56* (2), 175−287.

(23) Tripathi, L. N.; Mishra, C. P.; Chaubey, B. R. Luminescence in ZnS : La and ZnS : (Mn, La) Phosphors. *Pramana* **1982**, *19* (4), 385−398.

(24) Joicy, S.; Saravanan, R.; Prabhu, D.; Ponpandian, N.; Thangadurai, P. Mn $^{2+}$ Ion Influenced Optical and Photocatalytic Behaviour of Mn−ZnS Quantum Dots Prepared by a Microwave Assisted Technique. *RSC Adv.* **2014**, *4* (84), 44592−44599.

(25) Tian, Y.; Zhao, Y.; Tang, H.; Zhou, W.; Wang, L.; Zhang, J. Synthesis of ZnS Ultrathin Nanowires and Photoluminescence with Mn2+doping. *Mater. Lett.* **2015**, *148*, 151−154.

(26) Saavedra-Rodriguez, G.; Pal, U.; Sánchez-Zeferino, R.; Álvarez-Ramos, M. E. Tunable White-Light Emission of Co2+ and Mn2+ Co-Doped ZnS Nanoparticles by Energy Transfer between Dopant Ions. *J. Phys. Chem. C* **2020**, *124* (6), 3857−3866.

(27) Ahemen, I.; De, D. K.; Dejene, F. B.; Viana, B. White Light Tunable Emissions from ZnS: Eu3+ Nanophosphors over 330−465nm Excitation Range for White LED Applications. *Mater. Res. Express* **2016**, *3* (4), 045016.

(28) Khaidir, R. E. M.; Fen, Y. W.; Zaid, M. H. M.; Matori, K. A.; Omar, N. A. S.; Anuar, M. F.; Wahab, S. A. A.; Azman, A. Z. K. Optical Band Gap and Photoluminescence Studies of Eu 3+ -Doped

Zinc Silicate Derived from Waste Rice Husks. *Optik (Munich, Ger.)* **2019**, *182*, 486−495.
(29) Leng, J.; Xu, Y.; Chan, Y.; Wang, P.; Ryuzaki, S.; Okamoto, K.; Tamada, K. Tuning the Emission Colors of Self-Assembled Quantum Dot Monolayers via One-Step Heat Treatment for Display Applications. *ACS Appl. Nano Mater.* **2020**, *3* (4), 3214−3222.
(30) Yuan, X.; Zheng, J.; Zeng, R.; Jing, P.; Ji, W.; Zhao, J.; Yang, W.; Li, H. Thermal Stability of Mn2+ Ion Luminescence in Mn-Doped Core-Shell Quantum Dots. *Nanoscale* **2014**, *6* (1), 300−307.
(31) Kravtsova, A. N.; Budnik, A. P.; Tsaturyan, A. A.; Pankin, I. A.; Bugaev, A. L.; Soldatov, A. V. Temperature Effect on the Structure and Characteristics of Quantum Dots Based on ZnS. *Zh. Strukt. Khim.* **2017**, *58* (7), 1435−1441.
(32) Xing, G.; Feng, Y.; Pan, M.; Wei, Y.; Li, G.; Dang, P.; Liang, S.; Molokeev, M. S.; Cheng, Z.; Lin, J. Photoluminescence Tuning in a Novel Bi 3+ /Mn 4+ Co-Doped La 2 ATiO 6 :(A = Mg, Zn) Double Perovskite Structure: Phase Transition and Energy Transfer. *J. Mater. Chem. C* **2018**, *6* (48), 13136−13147.
(33) Velikov, K. P.; Van Blaaderen, A. Synthesis and Characterization of Monodisperse Core-Shell Colloidal Spheres of Zinc Sulfide and Silica. *Langmuir* **2001**, *17* (16), 4779−4786.
(34) Zhao, J. G.; Zhang, H. H. Hydrothermal Synthesis and Characterization of ZnS Hierarchical Microspheres. *Superlattices Microstruct.* **2012**, *51* (5), 663−667.
(35) Motlan; Zhu, G.; Drozdowicz-Tomsia, K.; McBean, K.; Phillips, M. R.; Goldys, E. M. Annealing of ZnS Nanocrystals Grown by Colloidal Synthesis. *Opt. Mater. (Amsterdam, Neth.)* **2007**, *29* (12), 1579−1583.
(36) Shahi, A. K.; Pandey, B. K.; Singh, B. P.; Gupta, B. K.; Singh, S.; Gopal, R. Photo Physical Studies of PVP Arrested ZnS Quantum Dots. *Electron. Mater. Lett.* **2017**, *13* (2), 160−167.
(37) Darbandi, M.; Thomann, R.; Nann, T. Single Quantum Dots in Silica Spheres by Microemulsion Synthesis. *Chem. Mater.* **2005**, *17* (23), 5720−5725.
(38) Mahjoub, M. A.; Monier, G.; Robert-Goumet, C.; Réveret, F.; Echabaane, M.; Chaudanson, D.; Petit, M.; Bideux, L.; Gruzza, B. Synthesis and Study of Stable and Size-Controlled ZnO-SiO_2 Quantum Dots: Application as a Humidity Sensor. *J. Phys. Chem. C* **2016**, *120* (21), 11652−11662.
(39) Yang, P.; Ando, M.; Taguchi, T.; Murase, N. Encapsulation of Multiple QDs into SiO_2Beads by Reflux without Degrading Initial Photoluminescence Properties. *J. Phys. Chem. C* **2010**, *114* (49), 20962−20967.
(40) Mao, L. H.; Zhang, Q. H.; Zhang, Y.; Wang, C. F.; Chen, S. Construction of Highly Luminescent CdTe/CdS@ZnS-SiO_2 Quantum Dots as Conversion Materials toward Excellent Color-Rendering White-Light-Emitting Diodes. *Ind. Eng. Chem. Res.* **2014**, *53* (43), 16763−16770.
(41) Dake, L. S.; Baer, D. R.; Zachara, J. M. Auger Parameter Measurements of Zinc Compounds Relevant to Zinc Transport in the Environment. *Surf. Interface Anal.* **1989**, *14* (1−2), 71−75.
(42) Trajić, J.; Kostić, R.; Romčević, N.; Romčević, M.; Mitrić, M.; Lazović, V.; Balaž, P.; Stojanović, D. Raman Spectroscopy of ZnS Quantum Dots. *J. Alloys Compd.* **2015**, *637*, 401−406.
(43) Carrillo-Torres, R. C.; Saavedra-Rodríguez, G.; Alvarado-Rivera, J.; Caldiño, U.; Sánchez-Zeferino, R.; Alvarez-Ramos, M. E. Tunable Emission and Energy Transfer in TeO2-GeO2-ZnO and TeO2-GeO2-MgCl2 Glasses Activated with Eu3+/Dy3+ for Solid State Lighting Applications. *J. Lumin.* **2019**, *212* (April), 116−125.
(44) Cristini-Robbe, O.; Raulin, K.; Dubart, F.; Bernard, R.; Kinowski, C.; Damene, N.; El Yazidi, I.; Boed, A.; Turrell, S. Porous Silica Supports for Micro-Raman Spectroscopic Studies of Individual Living Cells. *J. Mol. Struct.* **2013**, *1050*, 232−237.
(45) Brafman, O.; Mitra, S. S. Raman Effect in Wurtzite- and Zinc-Blende-Type ZnS Single Crystals. *Phys. Rev.* **1968**, *171* (3), 931−934.
(46) Vafayi, L.; Gharibe, S. Investigation of in Vitro Drug Release from Porous Hollow Silica Nanospheres Prepared of ZnS@SiOcore-Shell. *Bioinorg. Chem. Appl.* **2013**, *2013*, 1.
(47) Manca, M.; Cannavale, A.; De Marco, L.; Aricò, A. S.; Cingolani, R.; Gigli, G. Durable Superhydrophobic and Antireflective Surfaces by Trimethylsilanized Silica Nanoparticles-Based Sol-Gel Processing. *Langmuir* **2009**, *25* (11), 6357−6362.
(48) Kim, D.; Jin, Y.-H.; Jeon, K.-W.; Kim, S.; Kim, S.-J.; Han, O. H.; Seo, D.-K.; Park, J.-C. Blue-Silica by Eu2+-Activator Occupied in Interstitial Sites. *RSC Adv.* **2015**, *5* (91), 74790−74801.
(49) Perera, A. S.; Cockcroft, J. K.; Trogadas, P.; Yu, H.; Kapil, N.; Coppens, M. O. Titanium(IV)-Induced Cristobalite Formation in Titanosilicates and Its Potential Impact on Catalysis. *J. Mater. Sci.* **2019**, *54* (1), 335−345.
(50) Tang, C.; Zhu, J.; Zhou, Q.; Wei, J.; Zhu, R.; He, H. Surface Heterogeneity of SiO_2 Polymorphs: An XPS Investigation of α-Quartz and α-Cristobalite. *J. Phys. Chem. C* **2014**, *118* (45), 26249−26257.
(51) Pelmenschikov, A.; Strandh, H.; Pettersson, L. G. M.; Leszczynski, J. Lattice Resistance to Hydrolysis of Si - O - Si Bonds of Silicate Minerals: Ab Initio Calculations of a Single Water Attack onto the (001) and (111) β-Cristobalite Surfaces. *J. Phys. Chem. B* **2000**, *104* (24), 5779−5783.
(52) Effendy, N.; Aziz, S. H. A.; Kamari, H. M.; Matori, K. A.; Zaid, M. H. M. Enhanced Green Photoluminescence of Erbium Doped Zn 2 SiO 4 Glass-Ceramics as Phosphor in Optoelectronic Devices. *J. Alloys Compd.* **2019**, *783*, 441−447.
(53) Trukhin, A. N.; Smits, K.; Jansons, J.; Kuzmin, A. Luminescence of Polymorphous SiO_2. *Radiat. Meas.* **2016**, *90*, 6−13.
(54) McCamy, C. S. Correlated Color Temperature as an Explicit Function of Chromaticity Coordinates. *Color Res. Appl.* **1992**, *17* (2), 142−144.

https://doi.org/10.1021/acsanm.1c02689
ACS Appl. Nano Mater. 2021, 4, 12180−12187